Hydrogenated Carbon−Lead Films Plasma-Deposited from Tetraethyllead in a Three-Electrode Reactor

J. Tyczkowski* and B. Pietrzyk

Centre of Molecular and Macromolecular Studies, Polish Academy of Sciences, Sienkiewicza 112, 90-363 Lodz, Poland

M. Delamar

Institut de Topologie et de Dynamique des Systemes, Universite Paris VII, 1 rue Guy de la Brosse, 75005 Paris, France

Received April 27, 1998. Revised Manuscript Received September 21, 1998

Amorphous hydrogenated carbon−lead films (a-Pb_XC_Y:H) were produced by plasma chemical vapor deposition (PE CVD) in an audio-frequency (af) three-electrode reactor using tetraethyllead as a source compound. The negative amplitude of af voltage, $V_{(-)}$, measured on a small electrode, on which the films were deposited, with respect to the ground was the only operational parameter of the deposition process. $V_{(-)}$ was changed in the range of 0−1150 V. Investigations on electrical and optical properties, chemical structure, and morphology of the films were carried out. It has been found that a change in $V_{(-)}$ of about 100 V brings about rapid changes in the electrical conductivity (from 10^{-14} to 10^{-4} S/m), its activation energy (from 0.5 eV to the nonactivated process), and the optical gap (from about 3.0 to 1.3 eV). On the other hand, any drastic changes have not been observed in the chemical structure. This effect has been attributed to the amorphous insulator−amorphous semiconductor transition. It has been suggested that the transition effect is closely connected with the film cross-linking and Pb−C bonds play an important part in this process. The role of oxygen that is embedded into the film structures during the deposition process and the aging processes proceeding in the films under air treatment have been also discussed.

Introduction

Continuing our investigations on thin films produced by plasma chemical vapor deposition in a three-electrode reactor from organic compounds of the carbon family,[1−5] within this paper we deal with lead-containing films deposited from tetraethyllead. The three-electrode reactor was constructed a few years ago,[6−8] and it has proved a very useful system for production of semiconducting and insulating films from the same single-source precursor and in the same deposition process. It has been found, namely, that electronic properties of materials such as amorphous hydrogenated carbon−silicon (a-Si_XC_Y:H),[1] carbon−germanium (a-Ge_XC_Y:H),[2,3] and carbon−tin (a-Sn_XC_Y:H) films[5] strongly depend on a capacitance coupling two particular electrodes in the reactor. A very small variation of the capacitance in a defined range of its values brings about rapid changes in the dc conductivity (many orders of magnitude), the optical gap (more than 1 eV), and the transport gap (2−3 eV) of the deposited films. On the contrary, the basic chemical structure of the films, determined by chemical microanalysis, electron spectroscopies (both ESCA and Auger), and IR spectroscopy, is practically unchanged when the electronic structure reveals the step transformation. This amazing phenomenon has been attributed to a transition between amorphous insulator (a-I) and amorphous semiconductor (a-S) states.[3] It means that two qualitatively different materials, from the electronic structure point of view, are produced: typical amorphous semiconductors characterized by localized states forming only tails above and below the valence and conduction bands of extended states and so-called amorphous insulators in which all states are localized. The transition between them takes place when some critical degree of the short-range order in the deposited film is attained.[9−11]

Recent investigations on the deposition mechanism in the three-electrode reactor have shown that an ion bombardment process plays an important role in the

(1) Tyczkowski, J.; Kazimierski, P.; Odrobina, E. *Surf. Coat. Technol.* **1993**, *60*, 609.
(2) Tyczkowski, J.; Kazimierski, P.; Szymanowski, H. *Thin Solid Films* **1994**, *241*, 291.
(3) Tyczkowski, J.; Kazimierski, P. *J. Phys. D: Appl. Phys.* **1994**, *27*, 179.
(4) Tyczkowski, J.; Pietrzyk, B.; Szymanowski, H. *J. Chem. Vap. Depos.* **1996**, *4*, 261.
(5) Tyczkowski, J.; Pietrzyk, B.; Hatanaka, Y.; Nakanishi, Y. *Appl. Surf. Sci.* **1997**, *113/114*, 534.
(6) Tyczkowski, J.; Kazimierski, P.; Fallmann, W.; Olcaytug, F. Patent PL-169688B1, 1996.
(7) Tyczkowski, J.; Szymanowski, H.; Mazurczyk, R. *Surf. Coat. Technol.* **1997,** *98*, 1369.
(8) Tyczkowski, J.; Pietrzyk, B. In *Surface Enginnering Towards the 21st Century*; Binshi, X., Shining, M., Jiajun, L., Youli, Z., Eds.; China Machine Press: Shanghai, 1997; p 344.
(9) Adler, D. *Solar Energy Mater.* **1982**, *8*, 53.
(10) Overhof, H.; Thomas, P. *Electronic Transport in Hydrogenated Amorphous Semiconductors*; Springer-Verlag: Berlin, 1989.
(11) Tyczkowski, J. *Thin Solid Films* **1989**, *168*, 175.
(12) Tyczkowski, J. *J. Vac. Sci. Technol. A* **1999**, *March/Apr*, in press.

10.1021/cm980312p CCC: $15.00
Published on Web 12/01/1998

phenomenon under discussion.[7,12] With the rising value of the coupling capacitance, the energy delivered to the film surface by ions increases and a more and more advantageous thermodynamic system is obtained as far as the critical degree of the short-range order is surpassed. It should be emphasized, however, that basic plasma processes are absolutely independent of the coupling capacitance; thus, we can separately control the ion impact energy and the plasma chemistry in the reactor. Very often the coupling capacitance is used as the only operational parameter, with the rest of deposition parameters, such as initial pressure, flow rate, discharge power, and substrate temperature, remaining constant. In such a case we can trace the a-I−a-S transition effect for a material in which only the degree of short-range order is changed.

Apart from the fact that the a-I−a-S transition is an exciting effect, calling for further intensive investigations to understand its nature fully, the prospects of production of twin films characterized by semiconducting and insulating properties open a new thin film technology, e.g., preparation of a novel class of superlattice structures.[13,14] Amorphous hydrogenated carbon−lead alloys (a-Pb_XC_Y:H) complete the series of films consisting of elements belonging to the carbon family deposited in the three-electrode reactor , which has been unexplored. Our interest in this material seems, therefore, to be fully justifiable. The question is simple: can we observe the a-I−a-S transition effect in films deposited from organolead compounds or not? In this paper the electrical and optical properties as well as the molecular structure and morphology of the films produced from tetraethyllead are discussed.

As far as thin films deposited from organolead compounds by any of the familiar plasma methods are concerned, it should be noticed that very little attention has been paid to these materials to date. The first information, to our knowledge, was published in 1961.[15] In that short note a thin film preparation by electron impact decomposition of tetraethyllead was described. A typical glow discharge for plasma deposition of carbon−lead films was used 20 years later by Liepins et al.[16] and Tkatschuk.[17] In the former paper the films were produced from tetramethyllead and tetraethyllead, whereas in the latter one trimethylvinyllead was used. Unfortunately, neither of them dealt with the electrical and optical properties of the films.

Experimental Procedures

A model of the three-electrode reactor used for production of a-Pb_XC_Y:H films is sketched in Figure 1. The reactor has been modified[8] in comparison with that utilized before, in which the three electrodes were parallel.[6,7] In this system a small electrode, on which substrates are attached, is placed horizontally between two main perpendicular electrodes maintaining a glow discharge. The small electrode and the living main electrode are externally coupled by a variable capacitor. The gap between the main electrodes is 4.0 cm and their size

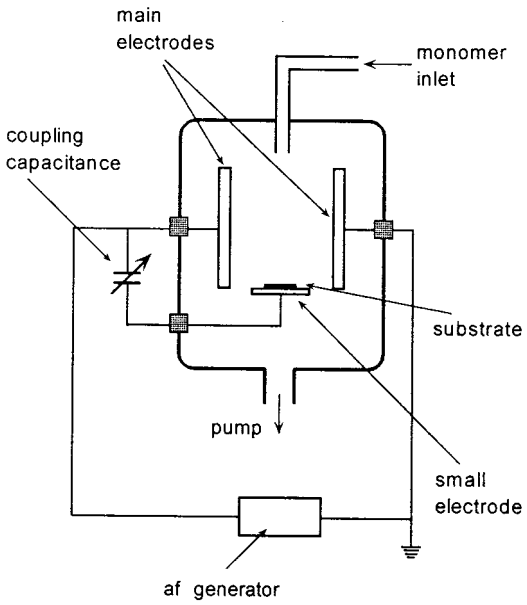

Figure 1. Schematic view of the three-electrode reactor used in this experiment.

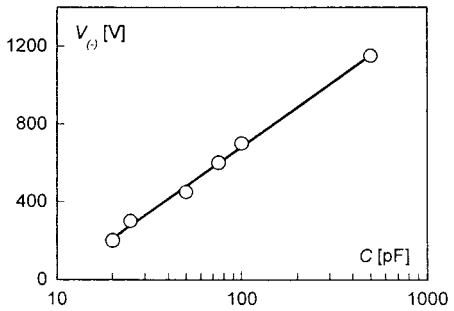

Figure 2. Dependence of the parameter $V_{(-)}$ on the coupling capacitance C for tetraethyllead plasma (frequency of 20 kHz, applied af voltage of 2400 V (peak-to-peak), flow rate of 0.45 sccm, and initial pressure of 13 Pa).

is 5.0 cm × 10.0 cm, whereas the area of the small electrode amounts to 2.5 cm × 6.0 cm. The reactor worked at a frequency of 20 kHz [audio-frequency range (af)] and with an applied af voltage of 2400 V (peak-to-peak). As already has been found, a more convenient and representative parameter than the coupling capacitance, C, including also the influence of other parameters on the ion bombardment process (e.g. the glow discharge power) and being directly proportional to the ion impact energy, is the negative amplitude of af voltage, $V_{(-)}$, measured on the small electrode with respect to the grounded electrode.[7,12] Therefore, all properties of the films under discussion are presented as functions of $V_{(-)}$. The negative amplitude, $V_{(-)}$, which was the only operational parameter in these studies, was controlled by C and was changed in the range of 0−1150 V. The dependence of $V_{(-)}$ on C for the glow discharge used in this work is shown in Figure 2.

The a-Pb_XC_Y:H films, 30−250 nm thick, were deposited from tetraethyllead [$(C_2H_5)_4Pb$], as a single source precursor, on 0.1 mm thick glass or quartz glass substrates. The flow rate of tetraethyllead vapor was 0.45 sccm, its initial pressure in the reactor chamber was 13 Pa, and the power supplied to the system was 17 W.

All measurements were performed in two general modes: for fresh samples exposed to air as briefly as possible and for the samples exposed to air at room temperature for 3−4 weeks. It was found that such aging was sufficient to obtain films with stable properties.

Measurements of dc electrical conductivity were carried out on samples in sandwich geometry (for films with conductivity lower than 10^{-10} S/m) and in coplanar geometry (for films with

(13) Silva, S. R. P.; Amaratunga, G. A. J.; Woodburn, C. N.; Welland, M. E.; Haq, S. *Jpn. J. Appl. Phys.* **1994**, *33*, 6458.
(14) Silva, S. P. R.; Rusli; Homewood, K. P.; Amaratunga, G. A. J. *J. Non-Cryst. Solids* **1998**, *227/230*, 1137.
(15) Baker, A. G.; Morris, W. C. *Review Sci. Instr.* **1961**, *32*, 458.
(16) Lepins, R.; Campbell, M.; Clements, J. S.; Hammond, J.; Fries, R. J. *J. Vac. Sci. Technol.* **1981**, *18*, 1218.
(17) Tkatschuk, B. W. *Vysokomolek. Soedin. B* **1982**, *24*, 232.

conductivity higher than 10^{-10} S/m). For the sandwich geometry, the films were deposited on the substrates with thermally evaporated gold strips forming the bottom electrodes. Gold top electrodes were evaporated perpendicularly to the bottom metal strips. The active electrode area was 0.04 cm^2. The coplanar geometry was formed by two parallel gold strips (0.1 cm apart and 1.0 cm long) evaporated on the films. Current−voltage and current−temperature dependences were measured in a vacuum (0.1 Pa) using a Keithley 617 programmable electrometer equipped with a voltage source. The specific conductivity was calculated from ohmic parts of the current−voltage characteristics.

Optical absorption measurements were performed by means of a Carl Zeiss Specord 40 spectrophotometer in the wavelength range from 200 to 900 nm using samples prepared on the quartz glass substrates.

The elemental composition and chemical constitution of the films were investigated by the X-ray photoelectron spectroscopy (XPS). A VG ESCALAB MK2 spectrometer with an Al Kα source (1486.6 eV) was used. The analyzed area was 600 μm. Binding energies were determined by attributing to the main C1s peak a value of 285.0 eV. The spectra were not subjected to smoothing. A Shirley-type baseline was calculated and signals were reconstructed using mixed peak shapes (typically 90% Gaussian and 10% Lorentzian). For composition calculations, the following relative elemental sensitivity coefficients were used: carbon, 1.0; oxygen, 2.65; and lead, 17.0. These coefficients were determined for our spectrometer using lead acetate crystals as a model system. Sputtering was performed with an Ar ion gun used in defocused mode in order to etch the whole sample surface (about 1 cm^2). XPS analyses were then performed at the center of the sample. Etching conditions were 5 kV ion energy and 400 μA ion current. Results from two successive etchings for a given sample were averaged.

The Pb concentration in the films was also determined by means of the quantitative chemical microanalysis method described by Marczenko.[18]

For scanning electron microscopy (SEM) and electron diffraction investigations, a JEOL JSH 35C scanning microscope and a Tesla TS 540 transmission electron microscope were used, respectively. For electron diffraction measurements the substrates were covered by a thin layer of KBr thermally evaporated before the film deposition. The films (30−40 nm thick) were separated from the substrates by treatment with water. Then, the films were carefully washed a few times in redistilled water, placed on microscopy meshes, and dried at room temperature. A typical diffraction measurement lasted up to 10−15 s with the electron beam density of 1.7×10^{23} s^{-1} m^{-2}. Modification of the film structure was performed by electron beam irradiation using the electron density of 1.5×10^{24} s^{-1} m^{-2} by a few minutes. The electron energy was 80 keV for both cases.

Experimental Results

Electrical Properties. Investigations of electrical conductivity of the a-Pb_XC_Y:H films constitute the first step toward the characterization of their electronic properties. Figure 3 presents such results (the dark conductivity σ measured at room temperature) for the films deposited at various values of the parameter $V_{(-)}$. As for other groups of films produced from organometallic compounds of the carbon family,[1−3,5] one can see in this case two kinds of materials as well: those with very low (10^{-14}−10^{-13} S/m) and those with high conductivity (10^{-5}−10^{-3} S/m). These two kinds of a-Pb_XC_Y:H films are also different in appearance. The low-conducting films are transparent and colorless while

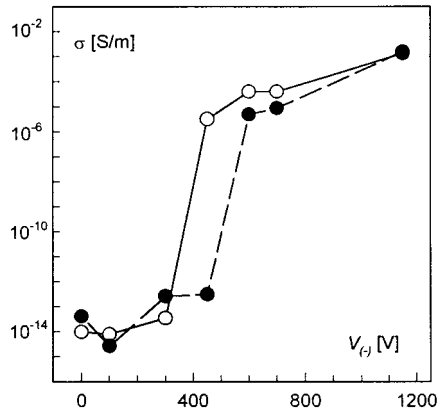

Figure 3. Electrical conductivity σ (measured at room temperature) of a-Pb_XC_Y:H films presented as a function of the parameter $V_{(-)}$: ○, fresh films; ●, aged films.

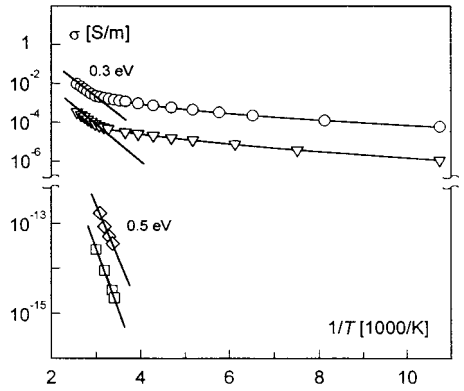

Figure 4. Dependence of the electrical conductivity σ on reciprocal temperature for the films prepared at various $V_{(-)}$: ○, 1150 V; ▽, 600 V; ◇, 300 V; □, 100 V.

the films with high conductivity are semitransparent and brown. It should be noted, however, that for the fresh films deposited in the medium range of $V_{(-)}$, i.e., between 300 and 600 V, the brown coloration decreases and σ drops after their exposure to air. The most evident changes are observed for $V_{(-)} = 450$ V. For the film produced at this value of $V_{(-)}$, after several weeks in air, the decolorization is complete and the conductivity changes from that of the high-conducting films to that typical for the low-conducting layers. This effect is responsible for a shift of the $V_{(-)}$ range, in which a transition from the material with low conductivity to that characterized by high electrical conduction can be observed: from 350−450 V (for films shortly after deposition) to 450−550 V (for aged films). It should be stressed, however, that the transition is very rapid in every case, and the change by many orders of magnitude in σ occurs when $V_{(-)}$ is changed only by more or less 100 V.

For better characterization of the electrical properties of the films under discussion, the temperature dependence of the conductivity was investigated. The results plotted in the Arrhenius coordinate system are presented in Figure 4. As one can see, the ln σ vs $1/T$ dependences for the low- and high-conducting films are quite different. In the case of the low-conducting films, although the temperature range of measurements is narrow, the dependence reveals a typical activation character, and the estimated activation energy is about 0.5 eV. The limits of the measuring range of tempera-

(18) Marczenko, Z. *Spectrophotometric Determination of Elements*; WNT and Ellis Horwood: London, 1976.

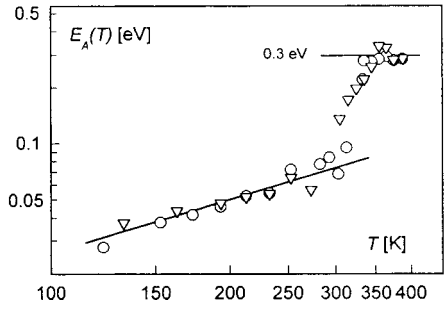

Figure 5. Double-logarithmic plot of the local activation energy $E_A(T)$ versus temperature for the high conducting a-Pb_XC_Y:H films: ○, film deposited at $V_{(-)} = 1150$ V; ▽, film deposited at 600 V.

ture in this case is caused, on one hand, by too low σ at lower T and, on the other hand, by the fact that σ irreversibly increases a few orders of magnitude at temperatures higher than 350 K.

On the contrary, the ln σ vs $1/T$ plots for the high conducting films consist of, apart from typical activation branches (with the activation energy of 0.3 eV), branches of a very weak temperature dependence. An effective method to demonstrate the character of such a dependence is a plot of the temperature-dependent activation energy, E_A, defined as the local gradient in the Arrhenius plot[19]

$$E_A(T) = k_B \frac{d[\ln \sigma(T)]}{d(1/T)} \tag{1}$$

where k_B is the Boltzmann constant. As shown in Figure 5, two regions can be distinguished in a double logarithmic plot of the local $E_A(T)$ against T. The first one corresponds to the activation process for $T > 330$ K (with $E_A \approx 0.3$ eV), and the second one represents the weak-temperature-dependent branches (for $T < 300$ K), revealing a good linear relationship. Such a relation allows us to attribute a hopping mechanism to the conductivity process that proceeds at temperatures below 300 K.[19]

It has been found that the hopping mechanism can be described reasonably well by the classic variable range hopping according to the relation[20]

$$\sigma = \sigma_0 T^{-1/2} \exp[-(T_0/T)^{1/4}] \tag{2}$$

where

$$\sigma_0 = \frac{3}{2} e^2 \nu_{ph} \left(\frac{N(E_F)}{2\pi\alpha k_B} \right)^{1/2} \tag{3}$$

and

$$T_0 \approx 16 \frac{\alpha^3}{k_B N(E_F)} \tag{4}$$

$N(E_F)$ is the density of states at the Fermi level, α is the inverse of the localization length, and ν_{ph} is the characteristic phonon frequency. Figure 6 presents the weakly temperature-dependent branches plotted according to relation 2. It should be emphasized that regardless of the equation that is used (eq 3 or 4) we can obtain, assuming $\alpha = 10^9$ m^{-1} and $\nu_{ph} = 10^{12}$ Hz, a very similar value of $N(E_F)$, equal to about 3×10^{25} eV^{-1} m^{-3}. Such a conformity between $N(E_F)$ values determined from the preexponential and the exponential factors is rather unique,[19,21] thus this result seems to be a strong argument for the variable range-hopping mechanism.

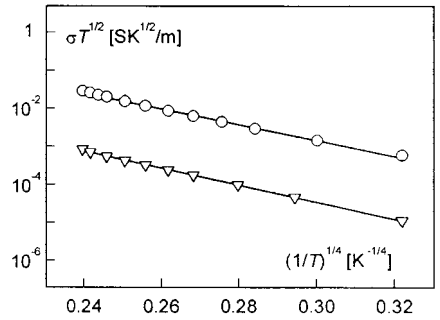

Figure 6. Data from Figure 4 given on a plot of $\log(\sigma T^{1/2})$ against $(1/T)^{1/4}$ according to the classic variable range hopping: ○ and ▽, films deposited at 1150 and 600 V, respectively.

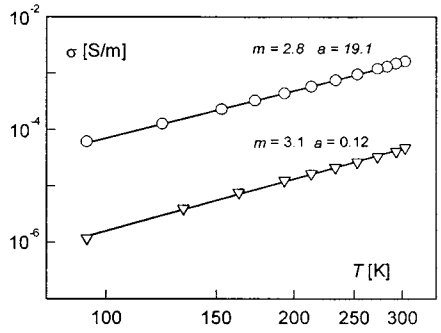

Figure 7. Data from Figure 4 given on a double-logarithmic plot of the conductivity σ versus temperature according to the multiple-phonon hopping. Related parameters a (in $[10^{-11}(S/m)(1/T)^m]$) and m (dimensionless) are given in the figure.

Recently, however, a lot of critical remarks have been made on the variable range hopping, and another alternative to this model, recognized as more satisfying to describe the weakly temperature-dependent processes, was developed. This is the multiple-phonon-hopping model.[19,22,23] In general, this process can be described by

$$\sigma = a T^m \tag{5}$$

where a and m are parameters. In Figure 7 the weakly temperature-dependent branches from Figure 4 are plotted according to this equation in the double-logarithmic coordinate system. The plots reveal very good linearity, and the quantities a and m can be directly obtained from these straight lines. They are shown in Figure 7. Both the values of the a and m parameters and their cross correlation seem to be quite realistic.[19]

Optical Properties. One of the most significant optical parameters of amorphous materials, which is

(19) Helmbold, A.; Hammer, P.; Thiele, J. U.; Rohwer, K.; Meissner, D. *Philos. Mag. B* **1995**, *72*, 335.
(20) Mott, N. F.; Davis, E. A. *Electronic Processes in Non-Crystalline Materials*, 2nd ed.; Oxford University Press: Oxford, 1979.
(21) Pramanik, M. K. A.; Islam, D. *J. Non-Cryst. Solids* **1981**, *45*, 325.
(22) Shimakawa, K.; Miyake, K. *Phys. Rev. B* **1989**, *39*, 7578.
(23) Shimakawa, K.; Kameyama, T. *J. Non-Cryst. Solids* **1989**, *114*, 786.

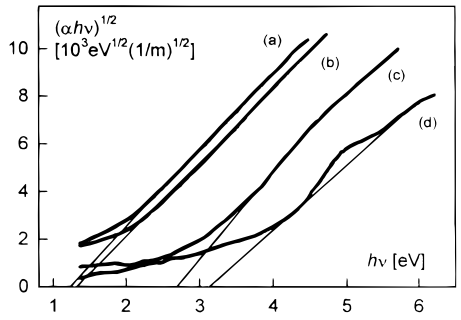

Figure 8. Absorption edges presented according to the Tauc relation (eq 6) for the following a-Pb_XC_Y:H films: (a) $V_{(-)}$ = 1150 V, fresh film; (b) $V_{(-)}$ = 1150 V, aged film; (c) $V_{(-)}$ = 0 V, fresh film; (d) $V_{(-)}$ = 0 V, aged film.

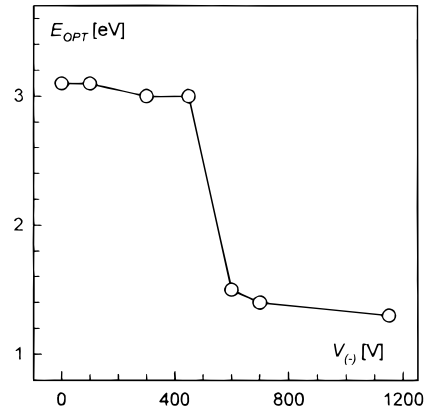

Figure 9. Optical gap E_{OPT} of the aged a-Pb_XC_Y:H films presented as a function of the parameter $V_{(-)}$.

related to their electronic structure, is the optical gap, E_{OPT}. Although this parameter has still no immediate physical meaning and there is some ambiguity about its experimental determination, it nevertheless is a useful quantity that allows comparison of samples with different electronic structures.[24] Most frequently E_{OPT} is estimated according to the Tauc relation[25]

$$\alpha h\nu = B(h\nu - E_{OPT})^2 \qquad (6)$$

where α is the absorption coefficient, $h\nu$ the energy of absorbed light, and B a proportionality factor.

The absorption edges for two typical films, representing the insulator and semiconductor groups, are plotted in Figure 8 according to eq 6. For the semiconducting film, the shape of the absorption edges for the fresh and aged films is almost the same, and E_{OPT} is equal to about 1.3 eV. On the contrary, the absorption edges for the insulating film before and after aging are different. E_{OPT} shifts from 2.7−2.8 eV to 3.0−3.1 eV and a new absorption band arises with a maximum at about 5.1 eV, for the aged film.

In Figure 9 E_{OPT} is presented as a function of $V_{(-)}$ for the aged films. As one can see, E_{OPT} changes rapidly from about 3.0 to 1.5 eV at the range of about 450−600 V. This range is identical as that where σ drops drastically (Figure 3).

Chemical Structure. The chemical structure of the a-Pb_XC_Y:H films has been examined by means of the XPS technique. Figure 10 shows an exemplary XPS spectrum (for the film deposited at $V_{(-)}$ = 1150 V). The origin of the particular lines is ascribed according to data from *Handbook of X-ray Photoelectron Spectroscopy*.[26] Three lines, namely C1s, O1s, and Pb$4f_{7/2}$, are taken into account for the further analysis of both the elemental composition and the chemical constitution.

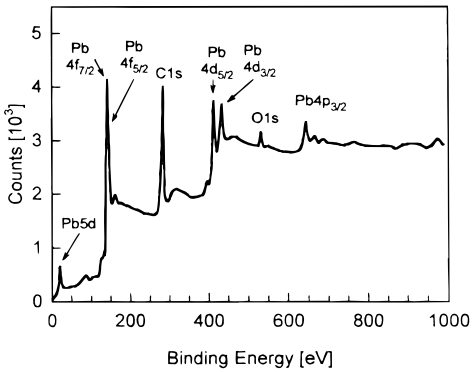

Figure 10. XPS spectrum of the aged film deposited at $V_{(-)}$ = 1150 V and subjected to cleaning by Ar^+ sputter etching.

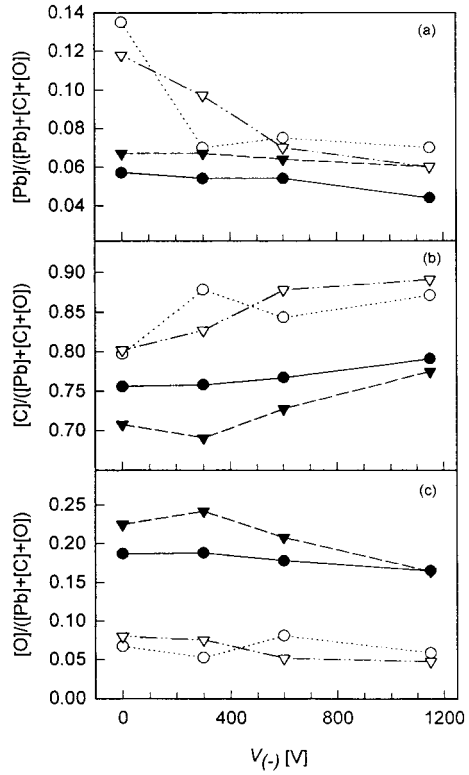

Figure 11. Elemental composition of surface (full symbols) and interior (open symbols) of the fresh (circles) and aged (triangles) films deposited at various $V_{(-)}$: molar fractions of (a) lead, (b) carbon, and (c) oxygen.

The elemental compositions of the surface and the interior of the films deposited with various $V_{(-)}$, both fresh and aged ones, are presented in Figure 11. The first important and surprising result is that the composition of the surface of the fresh films is almost identical for the semiconducting and insulating layers (full circles). After aging, an increase of the oxygen

(24) Bullot, J.; Schmidt, M. P. *Phys. Stat. Sol. (B)* **1987**, *143*, 345.
(25) Tauc, J. *Amorphous and Liquid Semiconductors*; Tauc, J., Ed.; Plenum Press: London, 1974, Chapter 4.
(26) Moulder, J. F.; Stickle, W. F.; Sobel, P. E.; Bomben, K. D. *Handbook of X-ray Photoelectron Spectroscopy*; Perkin-Elmer Corp., Physical Electronic Division: Minesota, 1992.

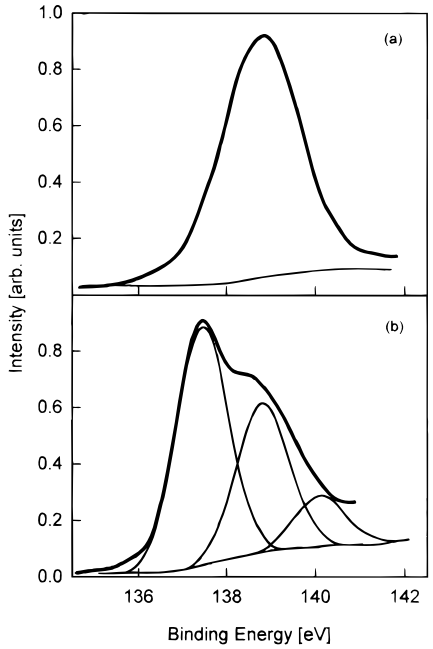

Figure 12. XPS spectra of Pb4f$_{7/2}$ core-level for surface (a) and interior (b) of an aged semiconducting a-Pb$_X$C$_Y$:H film ($V_{(-)}$ = 1150 V).

content, especially for the insulating films, occurs, but the molar fraction of Pb is practically unchanged in the entire range of $V_{(-)}$ (full triangles). It is generally known, however, that in many cases the surface analysis gives nonrepresentative results for the interior of materials. Therefore, the ion-etching process has been used to determine the interior elemental composition. Unfortunately, such a procedure may create a selective etching effect.[27] This process has turned out to be the only reasonable explanation of an increase in the Pb content visible in Figure 11a (from 0.07 to about 0.13). This increase is accompanied by a proportional decrease in the C content (Figure 11b). A chemical microanalysis performed for the films deposited at $V_{(-)} = 0$ V has shown, however, that Pb makes up only about 5 mol % in these films. Although the measuring error of this method is very high (±40%), the estimated value is absolutely much lower than the 13 mol % value obtained by the XPS measurements. It confirms our assumption that the selective etching effect occurs and it indicates that the lower $V_{(-)}$, the more effective the sputtering of carbon.

Taking into account the fact that the elemental composition of the film interior determined by XPS is slightly disturbed, mainly for the insulating films, by the selective etching effect, we can conclude that the real composition is almost identical within experimental error for all films deposited in the range of $V_{(-)}$, in which the drastic step changes in σ and E_{OPT} are observed. This composition is the following: Pb ≈ 7 mol %, C ≈ 87 mol %, and O ≈ 6 mol %.

To better understand the correlation between the chemical structure and the electronic properties, the chemical environments of Pb have been examined more thoroughly. In Figure 12 high-resolution Pb4f$_{7/2}$ spectra

(27) Kelly, R. *Handbook of Plasma Processing Technology*; Rossnagel, S. M., Cuomo, J. J., Westwood, W. D., Eds.; Noyes Publ.: Park Ridge, 1990.

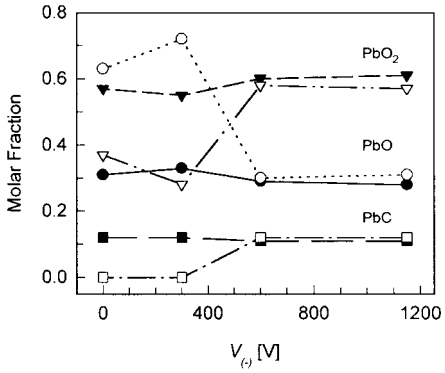

Figure 13. Molar fractions of Pb combinations (normalized to the constant Pb content) for the interior of the fresh (full symbols) and aged (open symbols) films deposited at various $V_{(-)}$.

Table 1. XPS Core Level Data for Various Pb Combinations

	binding energy Pb4f$_{7/2}$ [eV]		
Pb combination	measured	reported	refs
Pb−Pb		136.8−137.0	30, 38
PbO_2	137.4−138.3	137.2−138.3	31
PbO	138.8−139.2	138.2−139.2	30, 31, 39
PbC	140.1−140.5		

for the surface and the interior of the aged semiconducting film are shown. They are typical of all investigated films: only a single peak is recorded for the surface, whereas in the case of the interior the spectral envelope can be resolved into three peaks. The origin of the peaks is ascribed according to the published data (Table 1). Neutral Pb atoms have not been found in any film, which is indicative of a lack of Pb agglomerates in both the insulating and semiconducting films. As far as the surface of the films is concerned Pb occurs only in the form of PbO, both for the fresh and aged films. In the interior, however, we can distinguish three different types of Pb environments, namely PbO, PbO_2, and PbC. Their mutual relation is presented as a function of $V_{(-)}$ in Figure 13. As one can see, the molar fractions of the Pb environments are practically constant in the entire range of $V_{(-)}$ for the fresh films. After aging, the contents of these combinations in the semiconducting films are the same as those in the fresh samples. Pronounced changes, however, are observed for the insulating films. In this case PbC completely vanishes, the molar fraction of PbO_2 decreases, and the PbO content considerably grows. The fact that the changes in the composition are revealed only for the aging samples indicates that they are in fact connected with the aging processes but not with a bombardment-induced effect.[27]

Morphology. Investigations performed by means of SEM have shown that all the films under discussion are morphologically homogeneous down to the microscope resolution (about 50 nm). It has also been found, on the basis of electron diffraction measurements, that the films are amorphous. A typical diffraction pattern is presented in Figure 14a. However, conducting the diffraction experiment for a longer time, that is, exposing an investigated sample to a higher electron beam irradiation dose than that typically used for the single measurement, we can observe changes in the film morphology. As one can see in Figure 14b,c, a crystalline phase occurs in the film. Moreover, the structure of this

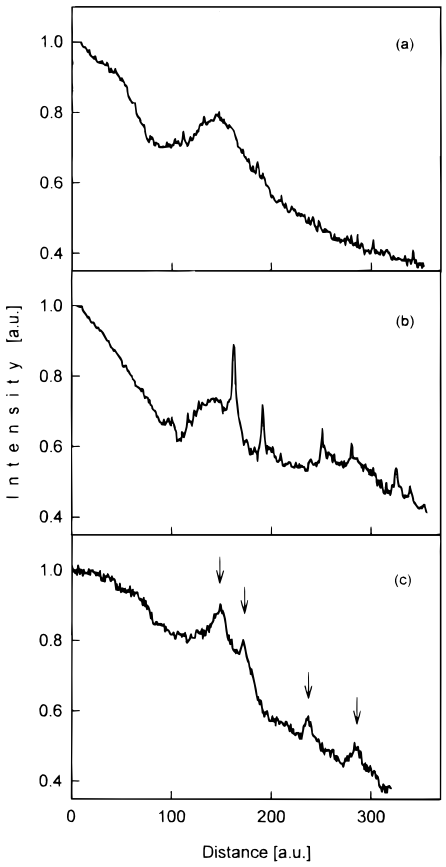

Figure 14. Electron diffraction patterns for a film deposited at $V_{(-)} = 1150$ V: (a) typical diffraction pattern, (b) after 2 min electron irradiation, (c) after 5 min electron irradiation.

Table 2. Electron Diffraction Data from Figure 14c in Comparison with Those for a Typical Lead Crystal

experiment		ASTM card Pb (cubic) 4-686	
d (nm)	I/I_0	d (nm)	I/I_0
2.87	100	2.855	100
2.49	40	2.475	50
1.76	25	1.750	31
1.49	30	1.493	32

phase transforms during electron beam irradiation, which is reflected by changes in the diffraction pattern.

The phenomenon of formation of a crystalline phase in amorphous materials upon electron beam irradiation has been already described for hydrogenated carbon−germanium films produced by plasma deposition in a three-electrode reactor.[28] It has been found that the crystalline phase of these films is composed of pure germanium nanocrystals. In contrast, the composition of the crystalline phase in our case is much more complex. Pure lead nanocrystals occur in the a-Pb_XC_Y:H films only after the long electron beam irradiation. This is concluded from Table 2, in which the quantitative electron diffraction data from Figure 14c are compared to the lattice parameters of a typical lead crystal. For shorter irradiation times, however, the crystalline structure is very complicated and difficult to determine. The line positions estimated from Figure 14b are not related to any expected crystalline structures, such as PbO, PbO_2, Pb_XO_Y, and Pb, of which lattice parameters are taken from the American Society for Testing and Materials (ASTM) catalog. Thus, the question of crystalline phase formation in the a-Pb_XC_Y:H films induced by electron beam irradiation is still open. This problem, however, strays from the subject of this paper and it will not be touched on further.

Table 3. Electronic Structure Parameters of the Films Deposited at the Three-Electrode Reactor

	insulator			semiconductor			
film type	σ (S/m)	σ_0 (S/m)	E_A (eV)	σ (S/m)	σ_0 (S/m)	E_A (eV)	refs
a-Si_XC_Y:H	10^{-19}	5×10^{-6}	0.8	10^{-8}	10^{-3}	0.3	1, 36
a-Ge_XC_Y:H	10^{-18}	2×10^{-3}	0.9	10^{-3}	30	0.26	2, 3
a-Sn_XC_Y:H	10^{-15}	0.3	0.85	10^{-2}	10^2	0.25	5
a-Pb_XC_Y:H	10^{-14}	5×10^{-6}	0.5	10^{-3}	10^2	0.3	this paper

Discussion

The results of electrical and optical measurements show evidently that drastic changes in the film's conductivity (σ) (Figure 3), activation energy (E_A) (Figure 4), and optical gap (E_{OPT}) (Figure 9) occur when $V_{(-)}$ surpasses a critical value (from 350 to 450 V for films shortly after deposition and from 450 to 550 V for aged films). This can indicate that the a-I−a-S transition probably takes place also in the case of the a-Pb_XC_Y:H films. Although the rapid change in electronic properties of the films under discussion is very similar to that observed for other films deposited in the three-electrode reactor, such as a-Si_XC_Y:H,[29] a-Ge_XC_Y:H,[3] and a-Sn_XC_Y:H,[5] some differences among them are apparent.

The first essential difference is related to E_A of the low-conducting films. As one can see in Table 3, where σ, E_A, and also σ_0 determined from the relation

$$\sigma = \sigma_0 \exp\left(\frac{E_A}{kT}\right) \tag{7}$$

are collected for various films deposited in the three-electrode reactor, E_A of the insulators, except the a-Pb_XC_Y:H films, is about 0.8−0.9 eV. For the a-Pb_XC_Y:H films, E_A is much lower and amounts to 0.5 eV. It seems also that σ_0 should be much higher, if dependence of an evident growth of σ_0 on the atomic number of the metalloid atom, which appears from Table 3, is supposed to be preserved.

The next difference between the a-Pb_XC_Y:H films and other films presented in Table 3 concerns the semiconducting materials. The electrical conductivity typical for the semiconductors is revealed by the high-conducting a-Pb_XC_Y:H films only at temperature higher than 330 K ($E_A = 0.3$ eV, $\sigma_0 = 10^2$ S/m). At lower temperatures the weakly temperature-dependent conductivity occurs (Figure 4). Although it is not clear at this moment which mechanism governs this process, namely the variable range hopping (Figure 6) or the multiple-phonon hopping (Figure 7), there is no doubt that this is a hopping mechanism.

Taking into account the discussion presented above, we can suggest that the a-Pb_XC_Y:H films reveal, as do the other films deposited from organic compounds of the carbon family, the transition from an amorphous insu-

(28) Tyczkowski, J.; Pietrzyk, B.; Mazurczyk, R.; Polanski, K.; Balcerski, J.; Delamar, M. *Appl. Phys. Lett.* **1997**, *71*, 2943.

(29) Tyczkowski, J. *Pol. J. Appl. Chem.* **1998**, *42*, 135.

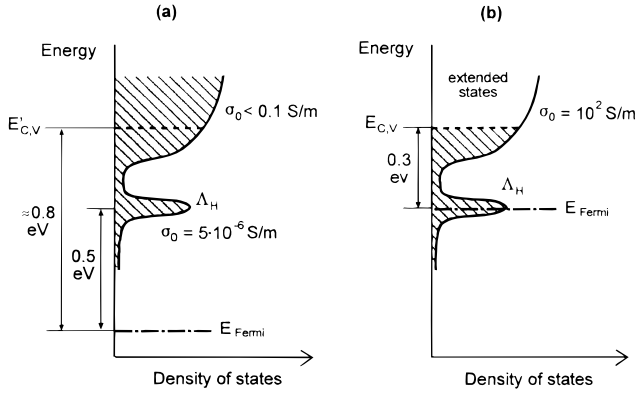

Figure 15. Models of density-of-states tails engaged in the conductivity processes for (a) insulating and (b) semiconducting a-Pb_XC_Y:H films.

lator to an amorphous semiconductor. This effect, however, is much more complex in this case due to additional transport states that do not exist in the other films. In Figure 15a,b models of the density-of-state tails engaged in the conductivity processes, for insulating and semiconducting a-Pb_XC_Y:H films, are presented. The conductivity of the insulator (see Figures 3 and 4) is connected with a hopping transport via states labeled as Λ_H. For all the other insulating films, in which Λ_H states have not been observed, the transport proceeds via band tail localized states lying at 0.8−0.9 eV from the Fermi level (Table 3). One can predict that such a process also takes place in our case, but its contribution to the whole conductivity is negligible. It has been found, calculated from eq 7, that σ_0 of this process is not higher than 0.1 S/m, which is a reasonable value compared to σ_0 for the other insulating films presented in Table 3.

If $V_{(-)}$ surpasses the critical value, the electronic structure of the a-Pb_XC_Y:H films is changed drastically (Figure 15b). In this case we can distinguish two transport processes. The first process, typical of the semiconducting films (see Table 3), consists of charge carrier transport via band tail states lying about 0.3 eV from the Fermi level. The parameter σ_0 of this process is about 10^2 S/m; that is at least 3 orders of magnitude higher than that related to the band tail transport in the insulating form of the films (0.1 S/m). Such a rapid rise in σ_0 can indicate that a change in the nature of the band tail transport process occurs, most likely a transition from the hopping transport in the insulating film to the extended state transport in the semiconducting film. The second transport process in the semiconducting a-Pb_XC_Y:H films, manifesting itself by the weakly temperature-dependent conductivity (Figure 4), is probably connected with the same Λ_H states as those in the insulating films. In this case, however, the Fermi level is pinned by these states, which explains the origin of the weak temperature dependence of conductivity.

The fact that the Λ_H states are observed only in the a-Pb_XC_Y:H films indicates that these states, from the molecular point of view, should be attributed to some Pb units. It seems that Pb−O groups could play such a role because they are present in the film structure, regardless of the film type. It is very difficult, however, to show precisely what kind of Pb connections creates the Λ_H states, because the two formal oxidation states of lead (Pb^{II} and Pb^{IV}) cannot be separately distinguished by XPS in mixed-valence oxide structures.[30,31]

Looking for the nature of the a-I−a-S transition, the main attention has also been paid to the chemical combinations of Pb. Although there is some basis to assume that the transition could be a result of changes only in carbon structures,[32] it should rather be rejected because films deposited from pure hydrocarbon in the same reactor and under the same conditions have not revealed any a-I−a-S transition effect.[4] As it has been found, the elemental composition and the molar fractions of the Pb units for the fresh films are practically constant in the entire range of $V_{(-)}$. Nevertheless, the drastic change in the electronic properties is observed at $V_{(-)} = 350-450$ V for such films. This result shows that a reason for the transition lies in some more refined changes in the molecular structure. The same conclusion has been already drawn from investigations performed on the other films deposited from organic compounds of the carbon family.[2,3,5] It has been suggested in that case that the a-I−a-S transition is connected with the short-range order in film structures and, in consequence, with the cross-linking of these structures.[29] Such an explanation can be also adopted to the films under discussion. The selective etching effect that has been found during the XPS measurements shows that the higher $V_{(-)}$ is, the higher the degree of the film cross-linking. With increasing cross-linking the degree of short-range order grows till it attains a critical value, causing the extended states to occur. In this moment the electronic structure of the film undergoes a drastic change, which is reflected by a shift of the Fermi level (about 0.5 eV) toward the transport band (Figure 15), the change of the charge carrier transport process, described above, and the narrowing of E_{OPT} by about 1.6 eV.

Considering the aging processes for the films deposited at intermediate $V_{(-)}$, that is from 300 to 600 V, one can conclude that Pb−C bonds play probably a significant role in the formation of the semiconducting form. The molar fraction of PbC is constant and independent of $V_{(-)}$ for the fresh films (Figure 13). In this case the transition a-I−a-S occurs at $V_{(-)} \approx 400$ V (Figure 3). For $V_{(-)} < 400$ V, the degree of short-range order is below its critical value, and despite the same concentration of PbC as that for higher $V_{(-)}$, only insulating films are produced. After aging, the PbC molar fraction decreases rapidly for $V_{(-)} < 600$ V. The lack of the PbC units in this region results in a shift of $V_{(-)}$, corresponding to the transition effect, to ≈500 V.

Another interesting observation emerging from analysis of the aging processes is a transformation of PbO_2 to PbO in the insulating films (Figure 13). The transformation is accompanied by the appearance of a broad absorption band at about 5.1 eV (Figure 8). Analogous bands have been found for various Pb systems such as amorphous lead halides[33−35] and lead monoxide.[36] This

(30) Evens, S.; Thomas, J. M. *J. Chem. Soc. Faraday II* **1974**, *70*, 313.
(31) Thomas, J. M.; Tricker, M. J. *J. Chem. Soc. Faraday II* **1974**, *70*, 329.
(32) Robertson, J. *Diamond Relat. Mater.* **1994**, *3*, 361.
(33) Kondo, S.; Marruyama, H.; Saito, T. *Phys. Stat. Sol. (A)* **1996**, *158*, 529.
(34) Kondo, S. *Phys. Stat. Sol. (A)* **1996**, *153*, 529.

latter system was produced by oxidation at room temperature of an evaporated thin Pb film. During the oxidation process, a very similar band, in shape and position, to that for the a-Pb_XC_Y:H films was recorded.

Generally, the absorption band under discussion can be attributed to the localized excitations of Pb^{2+} ions. It has been shown that the peak energy, E_0, of the band is nearly proportional to the squared inverse interionic distance, d, between Pb^{2+} and surrounding negative ions:[34]

$$E_0 = k/d^2 \qquad k \approx 0.4 \text{ nm}^2 \text{ eV} \tag{8}$$

On this basis, taking an assembly $Pb^{2+}O^{2-}$, which in fact can be attributed to PbO units, it has been calculated that E_0 (assuming the interionic distance is equal to 0.268 nm)[37] is about 5.5 eV. This is nearly the same value as that measured for the a-Pb_XC_Y:H films (Figure 8). It is also noteworthy that the broad shape of the band confirms the amorphous nature of the films.[34]

The aging process, manifesting itself by the transformation of PbO_2 to PbO and the cleavage of Pb−C bonds in the films deposited at $V_{(-)} < 600$ V, proceeds only under the influence of atmospheric air. In a vacuum all these reactions are stopped. It indicates that the aging process is a result of the action of atmospheric gases that have to diffuse into the film interior. Since any changes in the concentration of Pb combinations have not been practically observed in the semiconducting films ($V_{(-)} > 600$ V) under the influence of air (Figure 13), one can conclude that these films are much more cross-linked than those produced at $V_{(-)} < 600$ V. It confirms the foregoing thesis that the a-I−a-S transition is closely connected with the cross-linking degree of the films. Another conclusion emerging from these results is that oxygen in the fresh films, both semiconducting and insulating ones, originates rather from tail gases and it is built in film structures during the deposition process. The air treatment causes the further transformation in the structure only in the films deposited at $V_{(-)} < 600$ V, in which in-diffusion of atmospheric gases is possible.

Summary

The present study has proved that the a-Pb_XC_Y:H films deposited from tetraethyllead in the three-electrode reactor, similarly to other films produced from organic compounds of the carbon family, can be obtained as insulating or semiconducting materials, depending on the $V_{(-)}$ used as an operational parameter. The transition from insulating to semiconducting structures is closely connected with the cross-linking degree and, as a consequence, with the short-range order in the material. It is also suggested that Pb−C bonds play a crucial role in the transition process. If the degree of order is below its critical value or the concentration of Pb−C bonds is too low, only localized states exist in the transport bands and an amorphous insulator is created. In this case the transport of charge carriers proceeds via localized states Λ_H (laying about 0.5 eV from the Fermi level). It is suggested that these states can originate from Pb−O units. For the order degree higher than its critical value, extended states occur in the material and it can be classified as an amorphous semiconductor. Two different transport mechanism are proposed to explain the conductivity process in this case: transport via extended states laying about 0.3 eV from the Fermi level and a hopping transport via Λ_H states, which now overlap the Fermi level.

Generally, the passing of structures from insulating to semiconducting in the a-Pb_XC_Y:H films is connected with changes in electrical conductivity measured at room temperature from 10^{-14} to 10^{-4} S/m, in its activation energy from 0.5 eV to the thermally nonactivated process, and in the optical gap from about 3.0 to 1.3 eV.

As far as the parameter $V_{(-)}$ is considered, three groups of the a-Pb_XC_Y:H films can be distinguished: typical amorphous insulators (deposited at $V_{(-)} \leq 300$ V), typical amorphous semiconductors (deposited at $V_{(-)} \geq 600$ V), and films produced at 300 V $< V_{(-)} <$ 600 V, which are transformed from the semiconducting state to the insulating state as a consequence of the aging process. The fresh films belonging to the last group are characterized by a degree of cross-linking that ensures a sufficient degree of short-range order to make the semiconducting structure, but it does not protect against diffusion of atmospheric gases, giving rise to cleavage of Pb−C bonds. Thus, the electronic structure of the films converts into the insulating state.

Summarizing, the films deposited from tetraethyllead in the af three-electrode reactor reveal the a-I−a-S transition and confirm the general assumption of the presence of two types of plasma deposited films, namely amorphous insulators and amorphous semiconductors.

Acknowledgment. The authors wish to thank Dr. H. Szymanowski for performing the chemical microanalysis, Ms. E. Kmiecik and Mr. R. Mazurczyk for technical assistance, Mr. J. Balcerski from Physics Department of Lodz University for the diffraction examinations, and Dr. P. Kazimierski for his stimulating discussions. This work was partially supported by the KBN grant No. 3 T09A 022 15.

CM980312P

(35) Kondo, S.; Itoh, M.; Saito, T. *Phys. Stat. Sol. (A)* **1996**, *154*, 591.
(36) Tyczkowski, J.; Pietrzyk, B. Unpublished results.
(37) Kittel, C. *Introduction to Solid State Physics*, 6th ed.; John Wiley & Sons: New York, 1986.
(38) Powell, C. J. *Appl. Surf. Sci.* **1995**, *89*, 141.
(39) Terpstra, H. J.; deGroot, R. A.; Haas, C. *Phys. Rev. B* **1995**, *52*, 11690.